Journal of the Korean Physical Society, Vol. 73, No. 3, August 2018, pp. 302∼307

Effects of Structure and Sputtering Parameters on the Device Properties of Tin-Oxide Thin-Film Transistors

Han Byeol Seo
Department of NanoBio Tronics, Hoseo University, Asan 31499, Korea

Byung Seong Bae
Department of Display Engineering, Hoseo University, Asan 31499, Korea

Hyo In Bang and Eui-Jung Yun*
Department of ICT Automotive Engineering, Hoseo University, Dangjin 31702, Korea

(Received 21 February 2018, in final form 26 March 2018)

We investigated the device properties of sputter-deposited tin-oxide (SnO) thin-film transistors (TFTs) in which the SnO_x active layers were deposited by using a SnO sputtering target. The developed SnO-TFTs had a bottom-gate staggered or coplanar structure, which used a heavily-doped Si wafer as a gate electrode and 300-nm-thick SiO_2 as a gate dielectric layer. The TFTs with SnO_x thin-films deposited using a high radio-frequency (RF) power of 100 W, a very high working pressure of 20 mTorr, and an oxygen ratio of 0% revealed n-type characteristics. The coplanar SnO_x-based TFTs showed better n-type characteristics than the staggered ones, which was attributed to the good quality of the sputtered damage-free SnO_x films. On the other hand, the staggered TFTs with SnO_x deposited at a low RF power of 50 W, a low working pressure of 4 mTorr, and an oxygen ratio of 12% exhibited p-type characteristics, which included an onset voltage (V_{on}) of - 1.5 V, a saturated hole mobility of 39 cm^2/Vs at gate-to-source voltage (V_{GS}) = −10 V, a sub-threshold swing of 1 V/decade at $V_{GS} - V_{on} = -0.5$ V, and an on/off ratio of 1.1×10^2. We believe that our results can contribute to the development of p-type SnO-based TFTs with good performance.

PACS numbers: 73.21.Ac, 73.40.Qv, 73.61.Le, 85.30.De, 85.30.Tv
Keywords: Tin oxide (SnO) thin-film transistors, Sputter-deposited, p-type characteristics, High saturated hole mobility
DOI: 10.3938/jkps.73.302

I. INTRODUCTION

Recently, most oxide semiconductors (OSs) have been n-type. Therefore, OS-based thin-film transistors (TFTs) have been limited to the n-channel type. This is attributed to the fact that p-type OSs have low hole mobilities because their valence band maxima (VBM) are made mainly of anisotropic and strongly localized $2p$ orbitals of oxygen ions while n-type OSs have large electron mobilities because their conduction band minima (CBM) consist mainly of isotropic and delocalized s orbitals of metal cations [1–13]. Therefore, p-channel-type OS TFTs are still at the initial stage of research. Complementary metal-oxide semiconductor (CMOS) circuits, which offer great advantages over n-channel MOS (NMOS) circuits, specifically regarding power dissipation and higher density of logic functions on a chip, can be implemented if both n- and p-type oxide TFTs with well-controlled device parameters are realized [4, 5, 10, 14–20].

Recently, tin monoxide (SnO) has received particular attention because it is a good candidate for a p-type semiconductor with a large hole mobility due to its Sn $5s$ nature at the VBM [1–8, 10, 12, 13]. Here, we emphasize that the spatially spread and spherical Sn $5s$ orbitals, which hybridize and delocalize O $2p$ orbitals, are isotropic, resulting in high hole mobility. Until now, the characteristics of SnO-based TFTs have still been far from suitable for practical applications. Furthermore, at present, few reports in the literature demonstrate the effects of the sputtering process parameters and the structure on the properties of sputter-deposited SnO TFTs. Hence, in this study, we explored the device characteristics of bottom-gate staggered or coplanar TFTs with SnO active layers that had been fabricated by using a RF magnetron sputtering technique.

*E-mail: ejyun@hoseo.edu; Fax: +82-41-360-4859; Tel: +82-41-360-4855

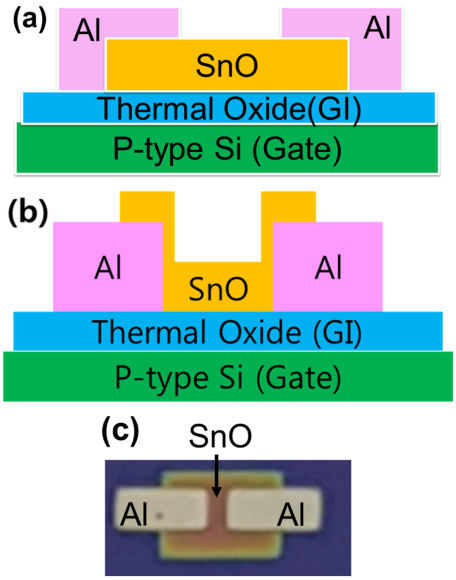

Fig. 1. (Color online) Schematic cross-sectional view of the bottom gate (a) staggered and (b) coplanar SnO TFT developed in this work and (c) photographic top view of typical bottom gate staggered SnO TFTs with $W = 1000$ μm and $L = 600$ μm.

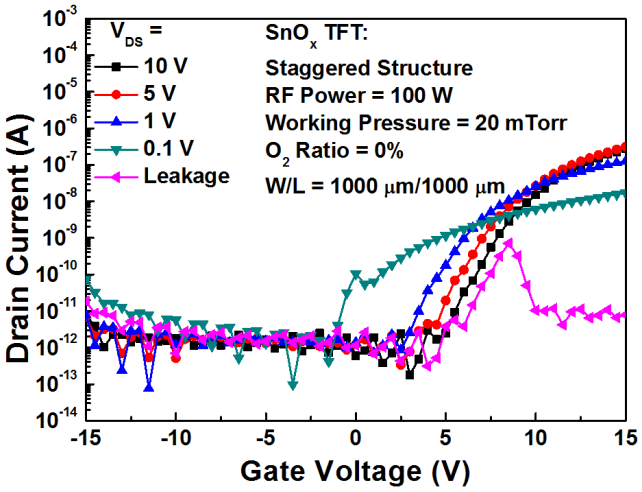

Fig. 2. (Color online) Typical I_{DS}-V_{GS} transfer characteristics for various values of V_{DS} for the bottom gate staggered TFTs with SnO_x films deposited at a RF power of 100 W, a working pressure of 20 mTorr, and an oxygen ratio of 0%. Samples had W/L dimensions of 1000 μm/1000 μm.

II. EXPERIMENTS

The fabrication process of TFTs is as follows: We fabricated two structures, the staggered and the coplanar structures. For the case of a bottom gate staggered configuration, the SnO_x active layer was deposited on a 300-nm-thick SiO_2 dielectric layer thermally-grown on a heavily-doped p-type Si gate electrode at room temperature (RT) by using a SnO sputtering target under the following conditions: radio-frequency (RF) powers of 50 - 100 W, working pressures of 4 - 20 mTorr, and oxygen ratios of 0 - 20%. Pure argon (99.999%) and oxygen gas mixtures were used as the reaction gas, and the total flow rate was 25 sccm. The target-to-substrate distance was kept constant at 10 cm for all depositions. The substrate was rotated at 13 rpm to deposit the SnO_x thin films with a uniform thickness. The SnO_x films' thicknesses were around 50 nm. Then, we prepared patterned 100-nm aluminum (Al) source and drain (S/D) electrodes on the top of the SnO active layers through a shadow mask by using a sputtering technique to fabricate the bottom gate staggered SnO TFTs. On the other hand, in the case of the bottom gate coplanar configuration, the SnO_x active layer was deposited after the preparation of patterned Al S/D electrodes although all deposition conditions were the same as those for the case of the bottom gate staggered one. The widths (W) and the lengths (L) of the samples were varied from 1000 to 1500 μm and from 650 to 1000 μm, respectively.

Figures 1(a) and 1(b) show schematic cross-sectional views of the bottom gate staggered and coplanar samples, respectively. Figure 1(c) shows a photographic top view of a typical bottom gate staggered sample with a W of 1000 μm and a L of 600 μm prepared in this study. For the prepared TFTs, the post-annealing was carried out at 423 K for 1 hr in a furnace in air before their device characteristics were measured. The device characteristics of the SnO-based TFTs were measured at room temperature in a darkened probe box in air by using two Keithley 2400 source meters for a DC voltage source and a Keithley 6485 picoammeter for current measurements along with the corresponding software (Microsoft visual basic). The capacitances of the SiO_2 gate dielectric films were measured at RT by using an Agilent 42854A precision LCR meter after having formed Ohmic contacts with a 100-nm-thick Al layer by using a sputtering technique.

III. RESULTS AND DISCUSSION

Figure 2 shows the typical drain-to-source current versus gate-to-source voltage (I_{DS}-V_{GS}) transfer curves of the bottom gate staggered TFTs with SnO_x active layers which had been prepared at a RF power of 100 W, a working pressure of 20 mTorr, and an oxygen ratio of 0%. The W/L dimension of the TFTs was 1000 μm/1000 μm. As shown in Fig. 2, the onset voltage (V_{on}), which is defined as the V_{GS} at which the mobile electron carriers start to accumulate in the channel and the I_{DS} starts to increase, was shifted positively from −1 to 5 V with increasing drain-to-source voltage (V_{DS}). This suggests that TFTs with staggered structure have instabilities induced by V_{DS}. We also noted that a positive V_{GS} was needed to accumulate the electron carriers in the n-type

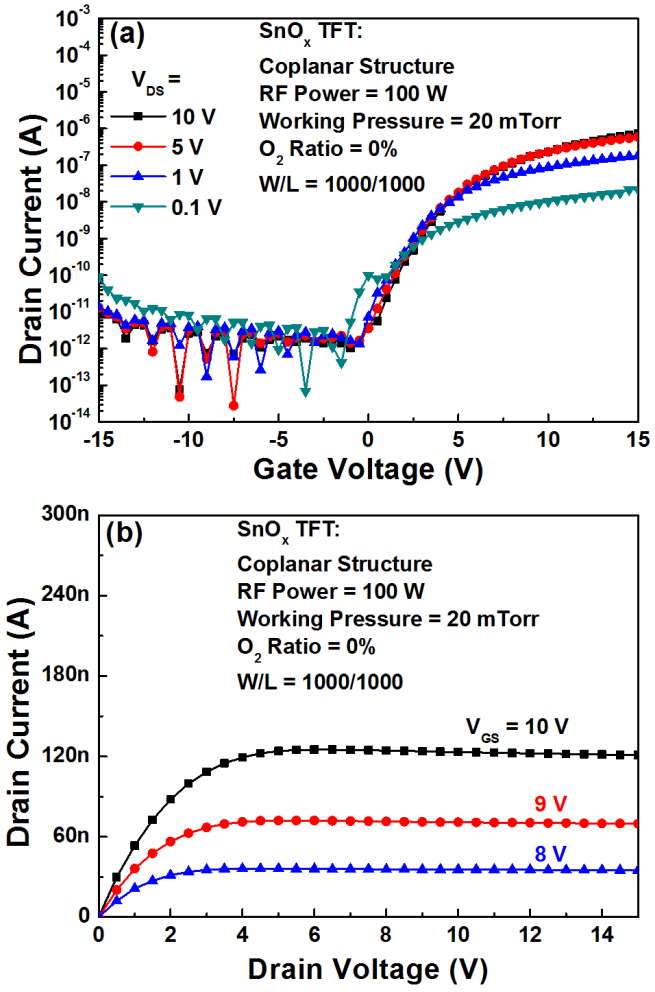

Fig. 3. (Color online) Typical (a) I_{DS}-V_{GS} transfer characteristics for various values of V_{DS} and (b) I_{DS}-V_{DS} output characteristics for various values of V_{GS} for the bottom gate coplanar TFTs with SnO_x films deposited at a RF power of 100 W, a working pressure of 20 mTorr, and an oxygen ratio of 0%. Samples had W/L dimensions of 1000 μm/1000 μm.

SnO_x active layer, which turns on the TFTs. This suggests that these TFT devices operate in the enhancement mode. Here, we believe that the high value of V_{DS} can contribute to an easy formation of an n-type channel in the SnO_x layer. We used the V_{on} rather than the threshold voltage (V_{th}) because the V_{on} is mainly determined by trapped charges whereas shifts in the V_{th} in the TFTs can be related to changes in many more physical parameters, such as the sub-threshold swing (SS) and the mobility [21,22].

To prepare TFTs with sputter-damage-free SnO_x, we fabricated the bottom gate coplanar TFTs, which have the same SnO_x deposition conditions and W/L dimension as those for the bottom gate staggered ones as shown in Fig. 2, and we show their transfer and output characteristics in Fig. 3. As shown in Fig. 3(a), the V_{on} was unchanged at approximately −1 V with increasing V_{DS},

Table 1. Summary of important device parameters of the sputter-deposited SnO-based TFTs with the bottom gate coplanar and staggered structures. The parameters were obtained from the transfer curves at V_{DS} = 10 V shown in Figs. 2 and 3. TFTs with coplanar structures showed better n-type properties than TFTs with staggered ones.

Sample description	On/off ratio	Saturation mobility [$cm^2/(V{\cdot}s)$]	SS (V/dec.)	V_{on} (V)
SnO-based TFTs with the bottom gate coplanar structure	6.9×10^5	5	0.8	−1
SnO-based TFTs with the bottom gate staggered structure	1.6×10^5	0.8	0.9	5

suggesting that the V_{DS} stability of TFTs with a coplanar structure is much better than that of TFTs with a staggered one. This better V_{DS} stability of TFTs with a coplanar structure was attributed to the good quality of the SnO_x films without sputtering damage. On the other hand, in the case of SnO_x TFTs with a staggered structure, the SnO_x active layer was damaged by the sputtering plasma during the Al S/D deposition, resulting in an increase in the number of oxygen vacancies within the SnO_x films, which in turn causes worse V_{DS} stability. In the case of the staggered structure, the overlapped area between the SnO_x active layer and the Al S/D electrodes was opened although the main part of active layer was shadowed by a metal shadow mask during the sputtering process for the Al S/D deposition, which caused a degradation of the opened SnO_x film's surface due to exposure to plasma bombardment. This caused a high contact resistance between the active layer and the S/D electrodes, resulting in the bad electrical characteristics of the staggered device. Furthermore, a microscopic gap existed between the active layer and the metal shadow mask due to the nature of the physical contact. This also caused the penetration of the plasma gas into the surfaces of the SnO_x films, which gave rise to bad device properties in the staggered TFTs.

Table 1 summarizes important device parameters, such as the SS, the field-effect saturation electron mobility ($\mu_{sat\text{-}electron}$), and the on/off drain current ratio, of the bottom gate SnO_x-based TFTs; the values of these parameters were obtained from the results in Figs. 2 and 3. The transfer curves measured at a V_{DS} of 10 V were used to extract the device parameters when the samples were operated in the saturation region. As listed in Table 1, the n-type characteristics of TFTs with a coplanar structure were better than those of TFTs with a staggered one. This confirms the aforementioned idea that the damage to the SnO_x active layers due to the sputtering plasma caused the worse n-type properties of TFTs with a staggered structure. We note that the samples showed n-type properties when the SnO_x active layer was deposited at a high RF power of 100 W,

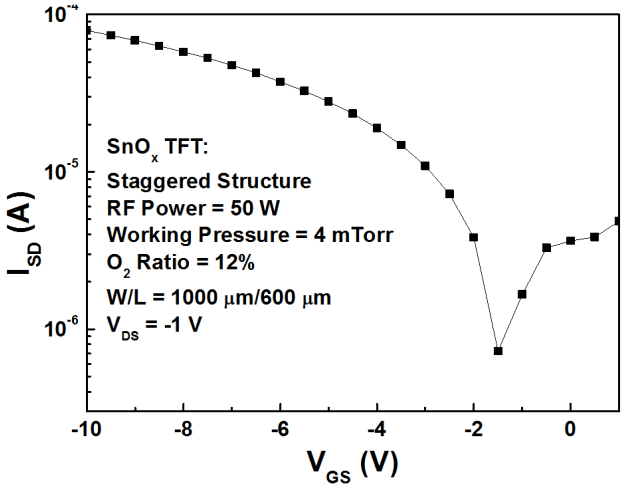

Fig. 4. Typical I_{SD}-V_{GS} transfer curve of a bottom gate staggered TFT with a SnO_x active layer prepared at a lower RF power of 50 W, a lower working pressure of 4 mTorr, and a higher oxygen ratio of 12% than the process conditions used in Figs. 2 and 3.

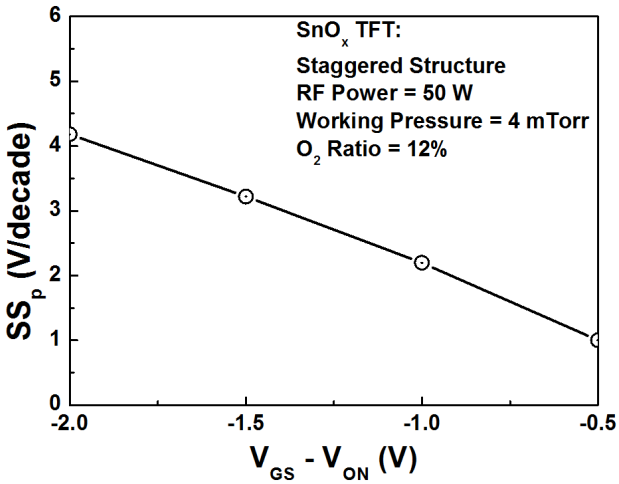

Fig. 5. Sub-threshold swing in p-type operation (SS_p) as a function of $V_{GS} - V_{on}$ estimated with Eq. (2) from the transfer curves for the sputter-deposited SnO TFTs shown in Fig. 4. The SS_p increases rapidly with increasing value of $|V_{GS} - V_{on}|$.

a very high working pressure of 20 mTorr, and a very low oxygen ratio of 0%. This suggests that the main phase of the active layer was SnO_2. Actually, we observed from dynamic secondary-ion mass spectrometry (D-SIMS) analyses (not shown) that the higher working pressure was the main factor for preparing more oxidized SnO_x films ($\sim SnO_2$). The gate valve was opened more to increase the working pressure of the chamber. Therefore, we believe that the higher working pressure caused the introduction of more oxygen atoms into the plasma in the chamber, which resulted in more heavily oxidized SnO_x films even at an oxygen ratio of 0%.

Figure 4 shows the typical source-to-drain current versus V_{GS} (I_{SD}-V_{GS}) transfer curves of the bottom gate staggered TFTs fabricated with SnO_x active layers that had been prepared at a lower RF power of 50 W, a lower working pressure of 4 mTorr, and a higher oxygen ratio of 12% than the process conditions used in Figs. 2 and 3. Worth mentioning is that all SnO_x active layers prepared at a low working pressure exhibited dominant Sn^{2+} X-ray photoelectron spectroscopy (XPS) peaks, indicating that SnO with p-type conductivity was the main constituent regardless of the oxygen ratio. As the oxygen ratio was increased to more than 12%, the Sn^{2+} XPS peak area percentage decreased while the Sn^{4+} XPS peak area percentage increased. This was attributed to a reduction in the SnO phase and the growth of the SnO_2 phase in the SnO_x active layers due to the incorporation of more oxygen. The W/L dimension of the TFTs was 1000 μm/600 μm, and the measurement was performed with the V_{DS} fixed at -1 V, which is in the saturation region. As shown in Fig. 4, samples revealed p-type characteristics. In Fig. 4, I_{SD} can be approximated as

$$I_{SD} \cong \frac{\mu_{sat\text{-}hole} W C_{\mathrm{SiO_2}}}{2L}(V_{GS} - V_{on})^2, \qquad (1)$$

where $\mu_{sat\text{-}hole}$ is the field-effect saturation hole mobility and $C_{\mathrm{SiO_2}}$ is the capacitance per area of the SiO_2 gate insulator, which was 11.5 nF/cm^2 as measured in a metal-insulator-metal configuration. V_{on} (~ -1.5 V) is defined as the negative V_{GS} at which the mobile hole carriers start to accumulate in the p-type SnO_x channel and the I_{SD} starts to increase, which turns on the p-type TFTs. Here, we emphasize that V_{on}, rather than V_{th} (~ -1 V), was used because the V_{on} is mainly determined by trapped charges whereas shifts in the V_{th} can be related to changes in many more physical parameters, such as the sub-threshold swing and the mobility. As shown in Fig. 4, the off-current level was found to be as high as 5×10^{-5} A. This high off-current level for our devices is attributed to the highly metallic nature of the SnO_x thin films due to the coexistence of metallic Sn phase defects in the SnO_x channel layer. We believe that the off-current level for the SnO_x TFTs decreases with decreasing metallic Sn more formed-phase defects in the SnO_x channel layer.

The sub-threshold swing in the p-type operation (SS_p), which describes the change in the V_{GS} that should be applied to devices in order to increase the I_{SD} by an order of magnitude, of the same devices used in Fig. 4 was also obtained from the inverse slope of the transfer curve shown in Fig. 4 by making use of [23,24]

$$SS_p = \left[\frac{d(\log I_{SD})}{d(V_{GS} - V_{on})}\right]^{-1}. \qquad (2)$$

The SS_p values extracted from the transfer curves shown in Fig. 4 by using Eq. (2) are shown in Fig. 5

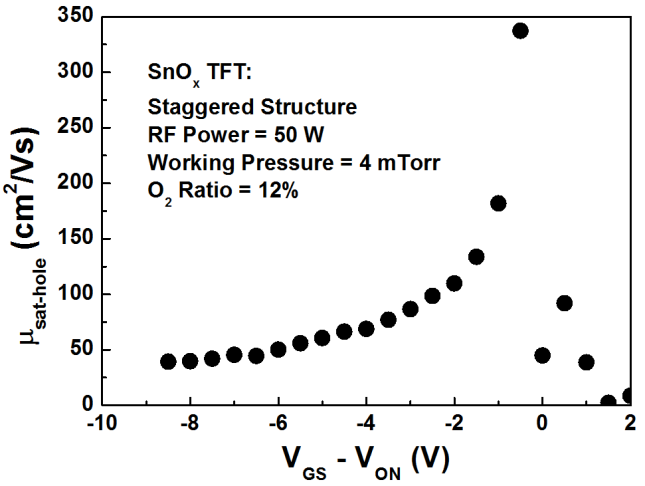

Fig. 6. Saturation hole mobility ($\mu_{sat\text{-}hole}$) at RT as a function of $V_{GS}-V_{on}$ estimated with Eq. (3) from the transfer curves for the sputter-deposited SnO TFTs shown in Fig. 4. The $\mu_{sat\text{-}hole}$ decreases rapidly with decreasing value of $V_{GS}-V_{on}$ from -1 to -10 V.

as a function of $V_{GS}-V_{on}$. In Fig. 5, the range of the value of $V_{GS}-V_{on}$ was limited between -2 and -0.5 because SS_p values were valid in this range based on the definition of SS_p which explains the change in the V_{GS} that causes a 10 times increase in the I_{SD}. As shown in Fig. 5, the SS_p values increase linearly with a slope of ~ 1.9 with increasing value of $|V_{GS}-V_{on}|$. An increase in the SS_p is known [25] to be related to an increase in the density of subgap trap states at the Fermi level (E_F) that are located close to the semiconductor/insulator interface. This indicates that higher defect densities can be induced easily at the SiO_2/SnO interface or in the SnO active layer by a higher value of $|V_{GS}-V_{on}|$. In these TFTs, we observed that the lowest SS_p value was around 1 V/decade at $V_{GS}-V_{on}=-0.5$ V, which increases up to 3.2 V/decade at $V_{GS}-V_{on}=-1.5$ V, as shown in Fig. 5. This also suggests that the sputter-deposited SnO-based TFTs developed in this study have a bad SnO/SiO_2 interface. We observed from atomic force microscopy analyses (not shown) that the surface roughnesses of SnO_x films increased with decreasing oxygen ratio from 12 to 0%, suggesting that the number of defects at the SiO_2/SnO interface increased as the oxygen ratio decreased. Therefore, the slope of the SS_p (shown in Fig. 5) is expected to increase with decreasing oxygen ratio.

The field-effect saturation hole mobility, $\mu_{sat\text{-}hole}$, was calculated using

$$\mu_{sat\text{-}hole}=\left(\frac{\partial\sqrt{I_{SD}}}{\partial(V_{GS}-V_{on})}\right)^2\frac{2L}{W}\frac{1}{C_{\mathrm{SiO_2}}}. \qquad (3)$$

Figure 6 shows $\mu_{sat\text{-}hole}$ versus $V_{GS}-V_{on}$, which was extracted from the transfer curve shown in Fig. 4 by using Eq. (3). The applied V_{GS} was adjusted by using the V_{on} to ensure that mobilities at various V_{GS} values could be accurately calculated [26]. As shown in Fig. 6, the saturation hole mobility decreases rapidly and saturates with decreasing the value of $V_{GS}-V_{on}$ from -1 to -10 V. A lower value of $V_{GS}-V_{on}$ below -1 V causes a higher hole carrier density in the SnO active layer, suggesting that carrier scattering occurs more frequently due to the participation of more hole carriers in scattering events, which leads to a rapid decrease in the $\mu_{sat\text{-}hole}$ value. Figure 6 also illustrates that the room-temperature $\mu_{sat\text{-}hole}$ is very high, around 337 cm^2/Vs at $V_{GS}-V_{on}=-0.5$ V, which decreases quickly down to 39 cm^2/Vs at $V_{GS}-V_{on}=-8.5$ V. Here, we emphasize that Eq. (1) and Eq. (3) are more sound physically for the saturation condition $V_{GS}-V_{on}\ll V_{DS}=-1$ V. This suggest that the very high $\mu_{sat\text{-}hole}$ of 337 cm^2/Vs at $V_{GS}-V_{on}=-0.5$ V is not realistic while the saturated $\mu_{sat\text{-}hole}$ of 39 cm^2/Vs at $V_{GS}-V_{on}=-8.5$ V is more reasonable.

Here, we report for the first time that the hole saturated mobility can decrease sharply and saturate to a relatively high value of 39 cm^2/Vs. We also concluded from the results in Figs. 4 - 6 that the TFTs with SnO channel layers prepared at a low RF power of 50 W, a low working pressure of 4 mTorr, and a high oxygen ratio of 12% revealed reasonable p-type characteristics in the enhancement mode, which included a saturated hole mobility of 39 cm^2/Vs at a $V_{GS}-V_{on}$ of -8.5 V, a SS_p of 1 V/decade at a $V_{GS}-V_{on}$ of -0.5 V, an on/off ratio of 1.1×10^2, and a V_{on} of -1.5 V.

IV. CONCLUSION

In this study, we investigated the device characteristics of bottom-gate staggered or coplanar TFTs with SnO active layers that had been fabricated by using a SnO sputtering target. The developed samples showed n-type properties when the SnO_x active layer was deposited at a high RF power of 100 W, a very high working pressure of 20 mTorr, and a very low oxygen ratio of 0%, suggesting that the main phase of the active layer was SnO_2. The V_{DS}-induced stability and n-type characteristics of TFTs with a coplanar structure were better than those of TFTs with a staggered one. These worse properties of TFTs with a staggered structure were attributed to an increase in the number of oxygen vacancies within the SnO_x films, which were damaged by the sputtering plasma during the Al S/D deposition. On the other hand, the TFTs with a SnO channel layer prepared at a low RF power of 50 W, a low working pressure of 4 mTorr, and a high oxygen ratio of 12% exhibited reasonable p-type properties in the enhancement mode, which included a saturated hole mobility of 39 cm^2/Vs at $V_{GS}-V_{on}=-8.5$ V, a SS_p of 1 V/decade at $V_{GS}-V_{on}=-0.5$ V, an on/off ratio of 1.1×10^2, and an V_{on} of -1.5 V. The samples with p-type characteristics had a bad SnO/SiO_2 interface with a

high defect density. The sharp decrease in the saturation hole mobility with increasing $|V_{GS} - V_{on}|$ for the p-type samples was associated with an increase in the number of carrier scatterings due to more hole carriers having been induced in the SnO by the higher $|V_{GS} - V_{on}|$.

ACKNOWLEDGMENTS

This research was supported by the Basic Science Research Program through the National Research Foundation of Korea (NRF) funded by the Ministry of Education (NRF-2016R1D1A3B03932570).

REFERENCES

[1] S-S. Lin, Y-S. Tsai and K-R. Bai, Appl. Surf. Sci. **380**, 203 (2016).
[2] S-S. Lin, S-Y. Fan and Y-S. Tsai, Ceram. Int. **43**, 1802 (2017).
[3] H-J. Kim, C-Y. Jeong, S-D. Bae, J-H. Lee and H-I. Kwon, IEEE Electron Device Lett. **38**, 473 (2017).
[4] L. Guo, M. Zhao, D. Zhuang, Q. Gong, H. Tan, M. Cao and L. Ouyang, Mater. Sci. Semicond. Process. **46**, 35 (2016).
[5] L. Qiang, W. Liu, Y. Pei, G. Wang and R. Yao, Solid-State Electronics **129**, 163 (2017).
[6] A. H-T. Nguyen, M-C. Nguyen, J. Choi, S. Han, J. Kim and R. Choi, Thin Solid Films **641**, 24 (2017).
[7] Y. Ogo, H. Hiramatsu, K. Nomura, H. Yanagi, T. Kamiya, M. Hirano and H. Hosono, Appl. Phys. Lett. **93**, 032113 (2008).
[8] L. Y. Liang, Z. M. Liu, H. T. Cao, Z. Yu, Y. Y. Shi, A. H. Chen, H. Z. Zhang, Y. Q. Fang and X. L. Sun, J. Electrochem. Soc. **157**, H598 (2010).
[9] K. Nomura, T. Kamiya and H. Hosono, Adv. Mater. **23**, 3431 (2011).
[10] E. Fortunato, P. Barquinha and R. Martins, Adv. Mater. **24**, 2945 (2012).
[11] J. Um, B. M. Roh, S. Kim and S. E. Kim, Mater. Sci. Semicond. Process. **16**, 1679 (2013).
[12] P. C. Hsu, W. C. Chen, Y. T. Tsai, Y. C. Kung, C. H. Chang, C. J. Hsu, C. C. Wu and H. H. Hsieh, Jpn. J. Appl. Phys. **52**, 05DC07 (2013).
[13] P. C. Hsu, W. C. Chen, Y. T. Tsai, Y. C. Kung, C. H. Chang, C. C. Wu and H. H. Hsieh, Thin Solid Films **555**, 57 (2014).
[14] R. Martins, A. Nathan, R. Barros, L. Pereira, P. Barquinha, N. Correia, R. Costa, A. Ahnood, I. Ferreira and E. Fortunato, Adv. Mater. **23**, 4491 (2011).
[15] C. Ju, C. Park, H. Yang, U. Kim, Y. M. Kim and K. Char, Curr. Appl. Phys. **16**, 300 (2016).
[16] J-H. Lee, Y-J. Choi, C-Y. Jeong, D-K. Jung, S. Ham and H-I. Kwon, IEEE Electron Device Lett. **37**, 295 (2016).
[17] A. Azmi, J. Lee, T. J. Gim, R. Choi and J. K. Jeong, IEEE Electron Device Lett. **38**, 1543 (2017).
[18] P-C. Chen, Y-C. Chiu, Z-W. Zheng, C-H. Cheng and Y-H. Wu, J. Alloys Compd. **707**, 162 (2017).
[19] H. Luo, L. Liang and H. Cao, Solid-State Electron. **129**, 88 (2017).
[20] J. S. Ahn, R. Pode and K. B. Lee, Thin Solid Films **608**, 102 (2016).
[21] M. Debucquoy, S. Verlaak, S. Steudel, K. Myny, J. Genoe and P. Heremans, Appl. Phys. Lett. **91**, 103508 (2007).
[22] J. K. Choi, J. M. Song, K. M. Yu, B. S. Bae and E. J. Yun, J. Korean Phys. Soc. **63**, 2281 (2013).
[23] D. C. Paine, B. Yaglioglu, Z. Beiley and S. Lee, Thin Solid Films **516**, 5894 (2008).
[24] K. M. Yu, J. T. Yuh, S. H. K. Park, M. K. Ryu, E. J. Yun and B. S. Bae, Jpn. J. Appl. Phys. **52**, 10MA12 (2013).
[25] T. Kamiya and H. Hosono, NPG Asia Mater. **2**, 15 (2010).
[26] C. G. Lee, B. Cobb and A. Dodabalapur, Appl. Phys. Lett. **97**, 203505 (2010).